Large anomalies due to insufficiency of Madelung embedding in *ab initio* calculations of 4*f*-5*d* and 4*f*-6*s* excitations of lanthanides in ionic crystals: The $BaF_2:Ce^{3+}$ crystal

José Luis Pascual,[1] Jöel Schamps,[2] Zoila Barandiarán,[3,4] and Luis Seijo[3,4,*]
[1]*Departamento de Química Física Aplicada, C-XIV, Universidad Autónoma de Madrid, 28049 Madrid, Spain*
[2]*Laboratoire PhLAM, Université de Sciences et Technologies de Lille 1, CERLA CNRS UMR 8523, F-59655 Villeneuve d'Ascq Cedex, France*
[3]*Departamento de Química, C-XIV, Universidad Autónoma de Madrid, 28049 Madrid, Spain*
[4]*Instituto Universitario de Ciencia de Materiales Nicolás Cabrera, Universidad Autónoma de Madrid, 28049 Madrid, Spain*
(Received 5 June 2006; published 11 September 2006)

Ab initio embedded-cluster calculations are performed on the $(CeF_8)^{5-}$ cluster embedded in BaF_2. The local structure around the Ce^{3+} impurity and the transition energies are calculated in the states of main character $4f^1$, $5d^1$, and $6s^1$, without and with spin-orbit coupling. When Madelung embedding is used, large anomalies are observed in the $5d^1$ and $6s^1$ manifolds. They are shown to be due to an artificial electron leak out of the cluster, at a regime of short Ce-F distances, when it occupies diffuse orbitals like the molecular orbitals of main character 5*d* and 6*s*. The main reason for the leak is the lack of linear-independency conditions between the wave functions of the cluster and its environment in Madelung embedding. When these conditions are added by means of *ab initio* model potential embedding (AIMP), the anomalies disappear. The 4*f*-5*d* absorption transitions calculated with spin-orbit coupling, AIMP embedding, and correlating the electrons with main character F-2*s*2*p* and Ce-4*d*5*s*5*p*4*f*5*d*, show good agreement with experiment. The present results support previous claims that state-of-the-art *ab initio* methods of quantum chemistry as the ones used here are nowadays in a position to reliably calculate 4*f*-5*d* transitions of lanthanide-doped solids. A proper embedding is crucial for this.

DOI: 10.1103/PhysRevB.74.104105 PACS number(s): 78.55.−m, 71.55.−i, 71.10.−w, 61.72.Bb

I. INTRODUCTION

The electronic excited states of lanthanide ions in ionic crystals with main configurational character $4f^{N-1}5d^1$ are very important from the basic and techonological points of view because of their involvement in a number of physical processes, ranging, e.g., from electronic Raman to solid-state lighting.[1–4] These states have been the subject of experimental studies for many years and their understanding is mainly supported by semiempirical models.[5–7] Theoretical methods based on the first principles might deliver significant contributions in this respect for two reasons: First, because they can provide sound analyses of interactions and effects involved in the processes,[8] and, second, because *ab initio* calculations that do not rely on empirical information can nowadays successfully simulate 4*f*-5*d* electronic spectra,[9] not only absorption spectra but also emission spectra. It is true, however, that carrying out these calculations to a good end is yet a difficult task.

It is known that for embedded-cluster *ab initio* calculations of local defects in ionic crystals to be reliable, the use of correct embedding potentials is a key question. In effect, it has been shown that taking a cluster made of an impurity and its first coordination shell in the solid, and embedding it in a large array of point charges (Madelung embedding), leads to unreasonable results in a number of cases, such as ground- and excited-state structures of high-symmetry defects,[10,11] Jahn-Teller stabilization energies,[12] and ionization and excitation energies of transition-metal ions in bulk ionic hosts,[13] as well as in chemisorption energies.[14] Moreover, all these results become meaningful after including embedding interactions of a quantum-mechanical nature between the solid lattice and the cluster, such as exchange and linear-independence (Pauli repulsion) interactions. However, the conclusions of these studies have not been fully spread and it is still common to find in the recent literature *ab initio* calculations on clusters embedded in arrays of point charges.

In this paper we show that, in the case of impurity states involving diffuse orbitals like the excited 5*d* and 6*s* orbitals of lanthanide ions, the inadequacy of Madelung embedding for a correct representation of the embedding effects can lead to dramatic anomalies in the predicted structural and spectroscopic properties of the impurity states. The anomalies are corrected when electrostatic embedding beyond the point-charge approximation and quantum-mechanical embedding (exchange and Pauli repulsion) are also included in an approximate way.

The calculations performed are *ab initio* model potential (AIMP) embedded-cluster calculations[10] of $4f \rightarrow 4f$, $4f \rightarrow 5d$, and $4f \rightarrow 6s$ local excitations of Ce^{3+}-doped BaF_2, carried out at the (wave-function based) complete active space self-consistent-field (CASSCF) (Ref. 15) and complete active space second order perturbation theory (CASPT2) (Refs. 16 and 17) level of dynamic electron correlation, and including scalar and spin-orbit coupling relativistic effects by means of relativistic effective core potentials.[18,19] The computed energies of the $4f \rightarrow 5d$ transitions show a good agreement with experiments when the correct AIMP embedding potentials are used. The breathing mode vibrational frequencies of the $4f \rightarrow 5d$ excited states are also computed and shown to agree well with the available experimental data.

The observed agreement with experimental data of $4f \rightarrow 5d$ excitations of $BaF_2:Ce^{3+}$ confirms previous agreements achieved in similar materials and transitions, such as

$4f$-$5d$ absorptions and emissions of $Cs_2NaYCl_6:Ce^{3+}$ (Ref. 9) and $5f$-$6d$ absorptions and emissions of $Cs_2ZrCl_6:Pa^{4+}$ (Ref. 20) and $Cs_2NaYCl_6:U^{3+}$ (Ref. 21). The present and the past agreements with experiments, together with the present demonstration of dramatic anomalies in Madelung embedded calculations of $4f \rightarrow 5d$ transitions, indicate that the use of point-charge embedding and the neglect of quantum-mechanical embedding effects (particularly Pauli repulsion) could be the reason for the large deviations from experiment obtained by Andriessen *et al.*[22] in a recent *ab initio* calculation on Ce^{3+} doped in BaF_2 and other ionic hosts, which led them to conclude that accurate *ab initio* calculations of $4f$-$5d$ excitations of lanthanides in ionic hosts are not possible, a conclusion that could have a negative impact on the growing interest for extracting very useful information out of *ab initio* calculations in these materials. Here it is shown that the use of a proper embedding is crucial in order to make the *ab initio* calculations accurate.

In Sec. II we summarize the method and the technical details. We present and discuss the results in Sec. III.

II. METHOD AND DETAILS OF THE CALCULATIONS

Ce^{3+} doped in BaF_2 creates local defects upon substitution of Ba^{2+} ions.[23] The charged defects created by this type of doping in fluorites can be locally compensated with interstitial fluoride ions[24] or nonlocally compensated with distant codoping ions like Na^+.[25] Although the effect of local compensations on the absorption and emission spectra is an interesting issue that will be the subject of further *ab initio* studies, the purpose of this paper is to claim the importance of a correct embedding and, here, we will only study the nonlocally compensated defect. It is an O_h cubic defect where the Ce^{3+} impurity is surrounded by a first coordination shell of eight F^- anions. We are interested in electronic states localized on the impurity which are involved in the absorption and emission spectra. These states are usually labeled with the main atomic orbital character of the open-shell electron and the O_h irreducible representations; neglecting spin-orbit coupling, they are the following: $4f^1$-$^2A_{2u}$, $4f^1$-$^2T_{1u}$, $4f^1$-$^2T_{2u}$, $5d(e_g)^1$-^2E_g, $5d(t_{2g})^1$-$^2T_{2g}$, and $6s^1$-$^2A_{1g}$. In the first three, the unpaired electron is in the inner $4f$ shell, which is very compact and shielded from the effects of the ligands by the outermost $5s$ and $5p$ filled shells. In the last three, the electron has crossed the $5s^25p^6$ barrier and occupies either the $5d$ shell, which is split by the ligands, or the $6s$ shell; the $5d(e_g)$, $5d(t_{2g})$ and $6s$ orbitals are all very diffuse and heavily exposed to the effects of the eight F^- ligands and of the rest of the BaF_2 host. Spin-orbit coupling splits further the levels and it is important for a fine interpretation of the spectra, but it can be safely neglected for bonding and structure issues, which are the focus here, as it has been shown in similar materials.[9,20,21] We will neglect spin-orbit coupling in most of the calculations and we will include it in a final calculation of the spectra of the cubic defect.

Although localized on the Ce^{3+} impurity, the local states are known to depend very much on the bonding interactions between Ce^{3+} and the surrounding F^- ions, as well as on the interactions between the $(CeF_8)^{5-}$ cluster and the rest of the host, and, accordingly, we will use an *ab initio* method that reliably takes into account (i) relativistic effects on Ce^{3+}, (ii) all bonding interactions within the $(CeF_8)^{5-}$ unit, and in particular a fair amount of dynamic electron correlations, and (iii) the embedding effects produced by the BaF_2 ionic lattice into the $(CeF_8)^{5-}$ cluster, not only of classical nature, but also of quantum-mechanical nature.

The *ab initio* method applied here results from a combination of techniques or methods of the quantum chemistry that specifically handle the above-mentioned effects. Bonding and correlation are taken care of with the multistate complete active space second-order perturbation theory method (MS-CASPT2),[16,17,26,27] which is a multireference many-body perturbation theory method, using molecular orbitals optimized with the complete active space self-consistent-field method (CASSCF).[15] Relativistic effects on Ce^{3+} are included by means of the use of effective core potentials calculated according to the *ab initio* model potential method (AIMP),[28] in its spin-free or scalar relativistic version based on Cowan-Griffin calculations[18,29] and in its spin-orbit coupling version based on Cowan-Griffin-Wood-Boring calculations.[19,30] Spin-orbit coupling and dynamic electron correlation effects are included together by means of the spin-free-state-shifted spin-orbit configuration interaction method (sfss-SOCI).[31] The AIMP method is also used as an embedding technique that includes classical and quantum-mechanical interactions between the $(CeF_8)^{5-}$ unit and the rest of the host.[10] All these methods have been described elsewhere and here we just summarize the technical details of the calculations; we make a more detailed description of the AIMP embedded-cluster Hamiltonian in order to facilitate the reading of the discussions. The present embedded-cluster calculations have been performed with the programs MOLCAS-6 (Ref. 32) (spin-orbit free calculations) and EPCISO (Ref. 33) (spin-orbit coupling calculations).

A. Embbeded-cluster Hamiltonian

The energies and many-electron wave functions of the local electronic states under consideration are calculated within the embedded-cluster approximation, with the following valence only, spin-orbit relativistic, AIMP embedded-cluster Hamiltonian for $BaF_2:(CeF_8)^{5-}$ (a detailed overall description in a general case can be found in Ref. 34):

$$\hat{H}^{AIMP}_{spin\text{-}orbit} = \hat{H}^{AIMP}_{spin\text{-}free} + \sum_{i=1}^{N^{clus}_{val}} \sum_{\mu \in clus}^{N^{clus}_{nuc}} \hat{h}^{spin\text{-}orbit}_{\mu}(i) + \sum_{\gamma} \delta_{\gamma} |\Phi^{\mathcal{P}}_{SF,\gamma}\rangle \times \langle \Phi^{\mathcal{P}}_{SF,\gamma}|, \quad (1)$$

where the the two last terms are the spin-orbit contribution and the spin-free-state-shifting term, which is a tool to put together spin-orbit coupling and large amounts of dynamic electron correlation (see Ref. 34 for full details). The first term, which is the most important one for the goals of this paper, is the scalar relativistic AIMP embedded-cluster Hamiltonian, which reads

$$\hat{H}^{AIMP}_{spin\text{-}free} = \sum_{i=1}^{N^{clus}_{val}} \left\{ -\frac{1}{2}\hat{\nabla}_i^2 + \sum_{\mu \in clus}^{N^{clus}_{nuc}} \left[-\frac{Z^{eff}_{\mu}}{r_{\mu i}} + \hat{V}^{AIMP}_{\mu\text{-}core}(i) \right] + \sum_{\xi \in host}^{N^{host}_{ion}} \hat{V}^{emb\text{-}AIMP}_{\xi\text{-}ion}(i) \right\} + \sum_{i=1}^{N^{clus}_{val}} \sum_{j>i}^{N^{clus}_{val}} \frac{1}{r_{ij}} + \sum_{\mu \in clus}^{N^{clus}_{nuc}} \sum_{\nu(>\mu) \in clus}^{N^{clus}_{nuc}} \frac{Z^{eff}_{\mu} Z^{eff}_{\nu}}{r_{\mu\nu}}. \quad (2)$$

In Eq. (2), the indices i and j refer to the N^{clus}_{val} valence electrons and μ and ν to the N^{clus}_{nuc} nuclei of the $(CeF_8)^{5-}$ cluster. Each nucleus μ of the cluster has N^{core}_{μ} core electrons and an effective nuclear charge $Z^{eff}_{\mu}=Z_{\mu}-N^{core}_{\mu}$; also, it has an effective core potential of the type AIMP, $\hat{V}^{AIMP}_{\mu\text{-}core}(i)$, which contributes the effects of the frozen core electrons and the scalar relativistic effects.

The classical and quantum-mechanical effects of the surrounding crystal are embodied in the AIMP embedding potential: the ξ sum of $\hat{V}^{emb\text{-}AIMP}_{\xi\text{-}ion}(i)$ terms of the Hamiltonian. The ξ index runs the N^{host}_{ion} embedding host ions, i.e., the ions of the doped material not included in the cluster, which in this case are all the ions of BaF_2:Ce^{3+} except the Ce^{3+} impurity and its first coordination shell of eight F^- ligands. The contribution of each host ion ξ reads[10]

$$\hat{V}^{emb\text{-}AIMP}_{\xi\text{-}core}(i) = -\frac{Q_{\xi}}{r_{\xi i}} + \frac{1}{r_{\xi i}} \sum_k C^{\xi}_k \exp(-\alpha^{\xi}_k r^2_{\xi i}) + \sum_j \sum_k |\chi^{\xi}_j\rangle A^{\xi}_{j,k} \langle \chi^{\xi}_k| + \sum_c D^{\xi}_c |\phi^{\xi}_c\rangle\langle\phi^{\xi}_c|. \quad (3)$$

The term $-Q_{\xi}/r_{\xi i}$ represents the long-range Coulomb potential created by a point charge Q_{ξ} (the ionic charge). The second term is the short-range Coulomb potential of the full ion which takes into account the spatial distribution of the electron charge density of the lattice ion to correct the point-charge potential. The last two terms represent, respectively, the full ion exchange operator and the full ion projection operator. These two terms stem from the first principles requirement of antisymmetry with respect to the interchange of electrons between cluster and embedding host.[35,36]

We should remark here the critical importance of the last term, $\Sigma_c D^{\xi}_c |\phi^{\xi}_c\rangle\langle\phi^{\xi}_c|$, because it is the term that prevents the cluster wave function from collapsing onto the lattice ion ξ. In this term, the ϕ^{ξ}_c are the occupied orbitals of the host ion ξ, and the projection constants D^{ξ}_c are taken to be minus twice their orbital energies, $D^{\xi}_c=-2\varepsilon^{\xi}_c$.[10,35,36]

As we said before, it is not uncommon to see embedded-cluster *ab initio* calculations performed on a simpler Madelung or point-charge embedding and here we will show some of the consequences of its use. The Madelung embedded-cluster Hamiltonian is obtained from the AIMP embedded-cluster Hamiltonian [Eq. (2)] after excluding short-range Coulomb and the quantum-mechanical terms:

$$\hat{H}^{Madelung}_{spin\text{-}free} = \hat{H}^{AIMP}_{spin\text{-}free} - \sum_{i=1}^{N^{clus}_{val}} \sum_{\xi \in host}^{N^{host}_{ion}} \left[\hat{V}^{emb\text{-}AIMP}_{\xi\text{-}ion}(i) + \frac{Q_{\xi}}{r_{\xi i}} \right]. \quad (4)$$

The AIMP embedding potentials for Ba^{2+} and F^- [Eq. (3)] have been obtained out of preparatory self-consistent embedded-ion calculations (SCEI) (Ref. 34) on BaF_2. In these, at a fixed geometry of the perfect BaF_2 crystal, Hartree-Fock (HF) calculations are performed on F^- and on Ba^{2+}, each of them embedded in BaF_2; with the orbitals and orbital energies of the F^- and Ba^{2+} ions, new embedding AIMPs are made and used to update the AIMP embedding potential of new HF calculations on embedded F^- and on embedded Ba^{2+}. This SCEI cycle is stopped when the results of two consecutive iterations converge within given thresholds. We used the experimental structure of BaF_2 (a_0 =6.2001 Å).[37] For F^-, we performed all-electron HF calculations with the Gaussian basis set $(8s5p)$ of Ref. 38 augmented with one p-type function from Ref. 39, contracted as $[4s4p]$. For Ba^{2+}, we performed effective core potential HF calculations, using the relativistic [Kr, $4d$] core CG-AIMP and $(10s10p)$ basis set of Ref. 18 contracted as $[6s6p]$.

The BaF_2 AIMP embedding potential used in the calculations of the embedded-cluster $(CeF_8)^{5-}$ was built in the following manner. First, embedding AIMPs of F^- and Ba^{2+} obtained in the preparatory SCEI calculations are located at experimental sites within a cube of edge $5a_0$ centered at the impurity (a total of 1656). An additional set of point charges is located at experimental sites within a cube of edge $8a_0$ (a total of 4888); of these, all ions bear the nominal ionic charge except those on the frontier faces, edges, and corners, for which Evjen's fractional charges are used[40] in order to accelerate the convergence of the Madelung potential. This procedure is led by the principle of making the potential-energy curves of the cluster stable under further improvement of the AIMP embedding potential of the host,[10] i.e., under additions of shells of embedding AIMPs and of shells of point charges. The embedding AIMPs, as well as other core AIMP data used in the paper (see below), are available from the authors.[41]

B. $(CeF_8)^{5-}$ wave functions and energies

The bonding interactions and dynamic electron correlation effects within the $(CeF_8)^{5-}$ cluster are accounted for with CASSCF+CASPT2 calculations. The complete active space (CAS) is defined with one electron in the molecular orbitals of main character Ce $4f$ (a_{2u},t_{1u},t_{2u}), Ce $5d$ (e_g,t_{2g}), or Ce $6s$ (a_{1g}), which means that the formal CASSCF calculations correspond to restricted open-shell SCF calculations. We will refer to the molecular orbitals by their main atomic orbital character all throughout the paper. The CASSCF wave functions are used as the zeroth-order reference for subsequent MS-CASPT2 calculations. Three different degrees of electron correlation are considered in three types of MS-CASPT2 culations: (i) Calculations labeled MS-CASPT2(F64, Ce1) take into account the dynamic correlation between the 65 valence electrons of $(CeF_8)^{5-}$ occupying the MOs of main character F $2s$ and $2p$ (64) and Ce $4f$, $5d$, or $6s$ (1). (ii) Calculations labeled MS-CASPT2(F64, Ce9) take into account the additional correlation of the eight electrons in Ce $5s$ and $5p$ orbitals. (iii) Calculations labeled MS-CASPT2(F64, Ce19) take into account the additional

TABLE I. Spectroscopic constants of cubic $(CeF_8)^{5-}$ embedded in BaF_2 as calculated at the spin-orbit free Hamiltonian level with Madelung embedding and AIMP embedding. R_e: Ce-F bond lengths, in Å; $\omega_{a_{1g}}$: breathing mode vibrational frequencies, in cm^{-1}; T_e: minimum-to-minimum excitation energies, in cm^{-1}.

	Shells of correlated electrons	Madelung embedding			AIMP embedding		
		R_e	$\omega_{a_{1g}}$	T_e	R_e	$\omega_{a_{1g}}$	T_e
$4f^1$-$^2T_{1u}$	none	2.589	307	0	2.510	357	0
	F-2*s*2*p*, Ce-4*f*	2.600	305	0	2.515	359	0
	F-2*s*2*p*, Ce-5*s*5*p*4*f*	2.560	301	0	2.479	355	0
	F-2*s*2*p*, Ce-4*d*5*s*5*p*4*f*	2.551	300	0	2.471	357	0
$4f^1$-$^2T_{2u}$	none	2.588	307	499	2.510	356	497
	F-2*s*2*p*, Ce-4*f*	2.599	304	475	2.514	359	472
	F-2*s*2*p*, Ce-5*s*5*p*4*f*	2.559	300	214	2.478	355	218
	F-2*s*2*p*, Ce-4*d*5*s*5*p*4*f*	2.552	301	18	2.472	357	14
$4f^1$-$^2A_{2u}$	none	2.594	309	1288	2.516	357	1569
	F-2*s*2*p*, Ce-4*f*	2.606	304	1254	2.520	360	1557
	F-2*s*2*p*, Ce-5*s*5*p*4*f*	2.567	301	1275	2.486	355	1628
	F-2*s*2*p*, Ce-4*d*5*s*5*p*4*f*	2.559	302	1359	2.479	357	1718
$5d^1$-^2E_g	none	2.358	426	26747	2.483	360	33913
	F-2*s*2*p*, Ce-5*d*	2.378	400	25122	2.476	364	29149
	F-2*s*2*p*, Ce-5*s*5*p*5*d*	2.346	411	24942	2.448	363	29899
	F-2*s*2*p*, Ce-4*d*5*s*5*p*5*d*	2.339	413	25795	2.441	364	31123
$5d^1$-$^2T_{2g}$	none	2.353	412	37711	2.542	356	49243
	F-2*s*2*p*, Ce-5*d*	2.374	391	35785	2.534	355	45691
	F-2*s*2*p*, Ce-5*s*5*p*5*d*	2.340	401	35413	2.507	354	47826
	F-2*s*2*p*, Ce-4*d*5*s*5*p*5*d*	2.331	403	36173	2.500	353	49473
$6s^1$-$^2A_{1g}$	none	2.345	412	32765	2.417	331	73779
	F-2*s*2*p*, Ce-6*s*	2.368	392	29929	2.404	348	63998
	F-2*s*2*p*, Ce-5*s*5*p*6*s*	2.333	401	29461	2.369	346	64382
	F-2*s*2*p*, Ce-4*d*5*s*5*p*6*s*	2.325	403	30231	2.363	344	65969

correlation of the ten electrons in Ce 4*d* orbitals. The sufficiency of the simple CAS used here and the necessity of correlating all the ligand valence electrons have been shown in calculations of Cs_2NaYCl_6:$(CeCl_6)^{3-}$ (Ref. 9) and Cs_2ZrCl_6:$(PaCl_6)^{2-}$ (Ref. 20). All the CASPT2 culations reveal large and uniform weights of the zeroth-order reference in all states calculated and show no sign of problems with intruder states.

In the sfss-SOCI calculations performed in order to compute spectra including spin-orbit coupling, only single excitations from the CAS have been used and the shifting parameters correspond to the MS-CASPT2(F64, Ce19) level of correlation.

C. Effective core potentials and Gaussian basis sets

For Ce, we use a [Kr]-core relativistic AIMP (active valence $4d,5s,5p,4f,5d,6s$ orbitals) and a $(14s10p10d8f)$ valence Gaussian basis set from Ref. 42. An additional set of three Gaussian primitive functions of *g* type, obtained by maximum radial overlap with the Ce^{3+} 4*f* orbital, is used for polarization. The final contraction of the Ce basis set is $(14s10p10d8f3g)/[6s5p6d4f1g]$. For F, we use a [He]-core relativistic AIMP (active valence $2s,2p$ orbitals) and the $(5s6p1d)$ basis set of Ref. 18, which includes one *p*-type diffuse function for anions[39] and one *d*-type polarization function.[38] The final contraction of the F basis set is $(5s6p1d)/[3s4p1d]$. The spin-orbit potentials were taken from Refs. 43 (Ce) and 44 (F).

III. RESULTS AND DISCUSSION

Table I shows the computed Ce-F bond lengths R_e breathing mode vibrational frequencies $\omega_{a_{1g}}$ and differences between the minima of energy curves T_e of cubic $(CeF_8)^{5-}$ embedded in BaF_2, as calculated at the spin-free Hamiltonian level, with AIMP embedding [Eq. (2)] and with the simpler Madelung embedding [Eq. (4)]. It shows results for the states of the $4f^1$, $5d^1$, and $6s^1$ configurations, where the unpaired electron occupies, respectively, the very compact 4*f* orbitals, which are shielded from the ligands by the more external $5s^25p^6$ filled shells; the 5*d* orbitals, which are more external than the filled shells, are quite diffuse and very exposed to the effects of the ligands; and the 6*s* orbital, which is a very diffuse one. In order to see the effects of different degrees and kinds of electron correlation, and how these can be af-

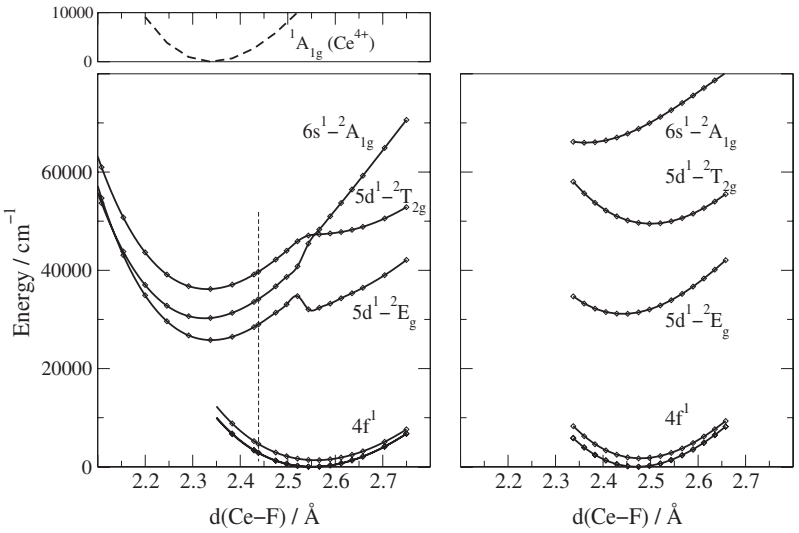

FIG. 1. Energy curves of several electronic states of cubic $(CeF_8)^{5-}$ embedded in BaF_2, calculated at the spin-free Hamiltonian level, with dynamic correlation of the electrons in the shells of dominant character F-2*s*2*p* and Ce-4*d*5*s*5*p*4*f*5*d*6*s*. Left: Madelung embedding calculations. Right: AIMP embedding calculations. The energy curve of the $^1A_{1g}$ ground state of BaF_2:$(CeF_8)^{4-}$ is shown in the up left box, with the same energy scale and the same distance values as the others.

fected by different embeddings, the table includes calculations at the mean-field level, with no correlation included, and at the MS-CASPT2 correlated level, with correlations of the 64 2*s* and 2*p* electrons of the fluorines plus several choices on the cerium ion: only the unpaired electron; this plus the 8 5*s* and 5*p* electrons; and these plus the 10 4*d* electrons. Although spin-orbit coupling is necessary for detailed discussions of spectroscopy, its effects on bonding are negligible and the bond lengths and vibrational frequencies in this table will not suffer significant changes upon its inclusion;[9,20,21] the excitation energies shift and split with spin-orbit coupling (see below), but the effects of correlation and embedding on them are basically independent of spin orbit and can be pinpointed in this table.

The most important physical effect of going from AIMP embedding to Madelung embedding is removing the linear-independence conditions that prevent the cluster wave functions from collapsing onto lattice ions. (Other effects are removing the short-range part of the Coulomb interactions and the exchange interactions between the cluster and its environment; they are less important, although not negligible.[34]) It is clear in Table I that not taking into account these embedding effects in the states of the $4f^1$ configuration leads to much longer bond lengths (around 0.08 Å) and much smaller vibrational frequencies (around 50 cm^{-1}), as a consequence of the additional artificial attraction towards the external ions experienced by the cluster electron density, which weakens the strength of the Ce-F bonds. This is the same anomaly that has been shown to happen in embedded clusters containing transition metals[10,12] and in the lanthanide series in a study of Ln^{3+}-doped Cs_2NaYCl_6.[11] The effect on the $4f^1$ intraconfigurational transition energies is not very large in absolute value (nevertheless, note a 20% increasing of the highest one). Also, for the $4f^1$ configuration, the sizes of the anomalies due to insufficiencies of Madelung embedding are not very different at different levels of treatment of correlation.

In the states of the $5d^1$ configuration of BaF_2: $(CeF_8)^{5-}$, using Madelung embedding leads to very different anomalies: very much shorter bond lengths (between 0.1 and 0.2 Å depending on the correlation level), much larger vibrational frequencies (between 40 and 60 cm^{-1}), and very much smaller 5*d* ligand field splittings (between 4500 and 8000 cm^{-1}), together with a much smaller value of the lowest $4f \rightarrow 5d$ transition (between 4000 and 7000 cm^{-1}). In this configuration the sizes of the anomalies depend much on the level of correlation. In the $6s^1$ configuration, the effects on bond lengths of an insufficient embedding are smaller than in the $5d^1$ configuration and the effects on vibrational frequencies are similar; however, the effects on the $4f \rightarrow 6s$ transitions are dramatic.

The reasons for the large anomalies observed in the $5d^1$ and $6s^1$ configurations can be better understood if we calculate not only the properties of the energy curves of the states at their respective equilibrium geometry, but also the energies of all the states in a wider range of Ce-F distances. The results are shown in Fig. 1. In the right-hand side box of this figure, where the AIMP embedding results are presented, we see smooth curves that show the same behavior previously found in $4f \rightarrow 5d$ (and $5f \rightarrow 6d$) excitations of *f*-element doped solids:[8] The $4f^N$ states are very parallel. The $4f^{N-1}5d^1$ configuration splits in two manifolds due to the ligand field splitting of the 5*d* orbitals, with the stabilized manifold having a shorter bond length than the $4f^N$ and the unstabilized manifold having a longer one. [See Ref. 8 for a detailed analysis of the reasons behind this observation. In brief: (i) The bond length ranges are dominated not by the size of the 4*f* and 5*d* orbitals, but by the size of the $5p^6$ shell, so that, if covalency, charge-transfer, and ligand field effects are removed, the bond lengths in $4f^{N-1}5d^1$ states are only slightly longer than in $4f^N$ states, contrary to what one would expect if attention is only paid to the size of the 4*f* and 5*d* orbitals. (ii) In $4f^{N-1}5d^1$ states, 5*d* covalency and charge transfer to the 4*f* hole shorten the bond lengths more than in $4f^N$ states; as a result the bond lengths of the average on configurations are either shorter in $4f^{N-1}5d^1$ than in $4f^N$, or very similar. (iii) Finally, the 5*d* ligand field splitting shortens further the stabilized manifold and elongates the unstabilized manifold, leading to the above described result.] Finally, the $6s^1$ state shows an even shorter bond length. The states of the $4f^{N-1}6s^1$ and $5f^{N-1}7s^1$ configurations of *f* element ions in solids are presently under study and will be the subject of future reports.

In the left-hand side box of Fig. 1, where the Madelung embedding results are shown, what we see, however, is the appearance of two distance regimes for the energies of the $5d^1$ and $6s^1$ states, with a sharp change of the energy curves between them. In the long-distance regime, the curves follow qualitatively the shape of the AIMP embedding results. In the short-distance regime, the three excited-state curves are fairly parallel. In the upper-left part of this figure, we have included the curve of the ground state of $(CeF_8)^{4-}$ in BaF_2 (using AIMP embedding), which corresponds to a Ce^{4+} impurity, and we can see that it is basically parallel to the $5d^1$ and $6s^1$ states of $(CeF_8)^{5-}$ embedded in BaF_2. This indicates that, in the Madelung embedding calculation, what we expected to be $5d^1$ and $6s^1$ states of $(CeF_8)^{5-}$ resulted in $(CeF_8)^{4-}$ plus one electron that has been spilled out of the cluster and does not influence the cluster equilibrium properties. This anomalous electron leak is caused by the removal of the linear-independency conditions, or Pauli repulsion, between the wave functions of the cluster and the environment, which is implicit in the simplification from AIMP to Madelung embedding, and makes the diffuse orbitals 5*d* and 6*s* to experience an abnormal additional attraction towards the cluster neigbhors; these orbitals are less repelled by the crystal anions and more attracted by the crystal cations than they should be. In the regime of long enough Ce-F distances, the 5*d* and 6*s* orbitals remain within the cage of the fluorine ligands, somehow shielded from the environment, and they only experience an artificial expansion. However, in a regime of sufficiently short Ce-F distances, which in this case seem to be shorter than 2.55 Å approximately, these diffuse orbitals have enough density outside the ligand cage so as to feel strongly the abnormal attraction by the environment, and they leak outside the cluster and collapse onto the crystal lattice.

In order to further support the previous explanation and to make it visible, we have drawn one of the e_g molecular orbitals with dominant character of Ce-5*d* in Fig. 2. The two lower boxes, which correspond to AIMP embedding in short (left) and long (right) Ce-F distance regimes, show that the orbital expands at short distances, when the covalency is larger. In the two upper boxes, where the orbital of the Madelung embedding calculation is shown, it is clearly seen that the electron has leaked out of the cluster in the short-distance regime.

Let us comment now on what sort of effects on the calculated ligand field splittings, energy centroids, and centroid shifts of the $5d^1$ configuration, we should expect from the insufficiencies of Madelung embedding. Having in mind that the main anomaly is a tendency to leak out in the short-distance regime, we must expect the effects to depend much on the basis set used, because some diffuse and very diffuse basis set functions that only play a secondary role at representing true molecular orbitals of 5*d* character, become the dominant ones when they have to represent an electron that is away from the cluster, collapsing onto external lattice sites. Also, in those calculations where the lanthanide-ligand distance is fixed in advance, the results should depend much on the chosen distance. In Table II we illustrate the effects we obtain with the technical details used in this paper. As we see, Madelung embedding leads to too small ligand field

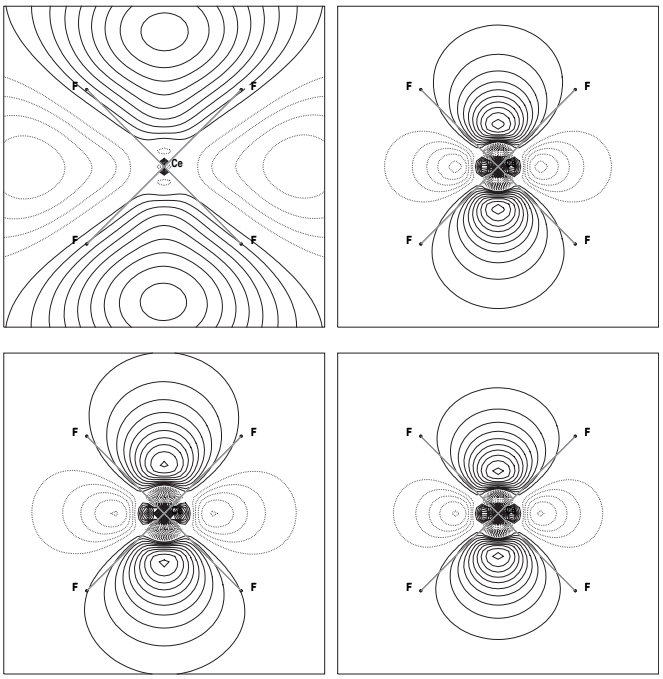

FIG. 2. Cross section (*xz* plane) of the MO of main character Ce-$5d(e_g)$ of cubic $(CeF_8)^{5-}$ embedded in BaF_2, which is occupied in the $5d^1$-^2E_g state. The eight F atoms are located at $(\pm 1, \pm 1, \pm 1) \times d(\text{Ce-F})/\sqrt{3}$. Above/below: Madelung/AIMP embedding calculations. Left/right: computed at $d(\text{Ce-F}) = 2.337$ Å/2.70 Å. Full lines are positive values and dotted lines are negative values; density increment between isolines is 0.025 in all cases.

splittings; this is in correspondence with an anomalous attraction of the negative charge of the ligands towards the host and far from the impurity, so lowering its effective charge (in a ligand field theory language). Also, Madelung embedding locates the centroid of the $5d^1$ configuration too low with respect to the $4f^1$ ground state and, as a consequence of this, the predicted centroid shifts with respect to the Ce^{3+} free-ion are too large. This is in agreement with the Judd-Morrison model for the centroid shift:[6,7,45] the anomalies lead to ligands with a higher polarizability, because of the lower concentration of charge, and to more diffuse 5*d* orbitals, both effects increasing the instant polarization of the ligands by the 5*d* electron which, according to the model, lowers the centroid energy of the $5d^1$ configuration with respect to the $4f^1$ ground state.

We must remark that the effects of correlation on the centroid shift are quite distorted when they are evaluated in Madelung embedding calculations. This is important because the ability to predict 4*f*-5*d* spectroscopic properties of materials is related to the understanding and prediction of centroid shifts and, according to the successful Judd-Morrison model,[6,7,45] the centroid shift is due to the different instant ligand polarization in the presence of 4*f* and 5*d* electrons, which is ultimately related to electron correlations within the cluster. In Table II we see that good agreements with experimental data on ligand field splitting, centroid, and centroid shift are achieved at the AIMP embedding level when F-2*s*2*p* and Ce-4*d*5*s*5*p*4*f*5*d* electrons are correlated. The

TABLE II. Ligand field splitting, energy centroid, and centroid shift of the $5d^1$ configuration of $BaF_2:(CeF_8)^{5-}$. All numbers in are cm^{-1}.

	Madelung embedding			AIMP embedding			Ce^{3+}
Correlated electrons[a]	$\Delta(5d)$[b]	$E(5d^1)_{ave}$[c]	$\Delta E(5d^1)_{ave}$[d]	$\Delta(5d)$[b]	$E(5d^1)_{ave}$[c]	$\Delta E(5d^1)_{ave}$[d]	$^2F \rightarrow {}^2D$
none	10964	33325	10270	15330	43111	490	43600
Ce-4f5d	10663	31520	12080	16542	39074	4520	43600
Ce-5s5p4f5d	10471	31225	13130	17927	40655	3700	44360
Ce-4d5s5p4f5d	10378	32020	14530	18350	42133	4420	46551
					experiment		
				19200[e]	43300[f]	6400[e]	49940[g]

[a]The F-2s2p electrons have also been correlated in the embedded-cluster calculations.
[b]Ligand field splitting defined as $\Delta(5d)=E_{min}(^2T_{2g})-E_{min}(^2E_g)$.
[c]Energy centroid of the $5d^1$ configuration of $BaF_2:(CeF_8)^{5-}$ with respect to the ground state, defined as $E(5d^1)_{ave}=[2/5E_{min}(^2E_g)+3/5E_{min}(^2T_{2g})]-E_{min}(^2T_{1u})$.
[d]Centroid shift with respect to the Ce^{3+} free ion, defined as $\Delta E(5d^1)_{ave}=E(Ce^{3+},{}^2D)-E(Ce^{3+},{}^2F)-E(5d^1)_{ave}$.
[e]Reference 45.
[f]Reference 24.
[g]Reference 50.

2000-cm^{-1} error in the centroid shift is mainly due to errors in the calculations of the centroid of the free ion, which is in line with the common experience that free ions are computationally more demanding than embedded ions, in terms of correlation and basis sets.[46,47] At the mean-field level, with no correlation included, the ligand field splitting is too small and there is a fortuitous agreement with experiment in the centroid as the result of error compensations; at this level, the centroid shift is only a small fraction of experiment, in agreement with the model.

Finally, we show in Table III the vertical absorption transitions calculated from the equilibrium structure of the ground state, with AIMP embedding and using the full spin-orbit Hamiltonian. They can be compared with the maxima of experimental absorption bands.[23] The experiments correspond to a C_{4v} defect, where the symmetry reduction from O_h is due to local charge compensation, so that we make the comparison here having in mind that the goal of this paper is not a detailed discussion of these experiments, but an analysis of the consequences of the use of a Madelung embedding. In any case, we can expect the effects from the local charge compensation to be, basically, a splitting of some levels of the cubic defect, so that a direct comparison between our results and the experiment is meaningful. What we see is a very good agreement. In addition to excitation energies, we can also compare the computed vibrational frequency of the breathing mode with the experiment in the lowest $5d^1$ state. We get 364 cm^{-1}, which is very close to the 360 cm^{-1} reported by Loh[23] for the totally symmetric frequency, out of the 0-0 (33 780 cm^{-1}), 0-1 (34 140 cm^{-1}), and 0-2 (34 500) lines of the vibrational progression in the lowest $4f \rightarrow 5d$ absorption. Let us also remark that Loh identified a very weak band in $CaF_2:Ce^{3+}$ peaking at 70 000 cm^{-1} as a $4f \rightarrow 6s$ transition; our value of 70 080 cm^{-1} for the $4f \rightarrow 6s$ transition in $BaF_2:Ce^{3+}$ fully supports his assignment.

TABLE III. UV absorption spectrum of Ce^{3+}-doped BaF_2. This work: vertical transitions from the equilibrium structure of the ground state, $4f^1$-Γ_{8u} (64.4% $^2T_{1u}$+35.6% $^2T_{2u}$), of the cubic cluster $(CeF_8)^{5-}$ embedded in BaF_2, calculated with spin-orbit coupling and AIMP embedding. Experiment: Manthey's interpretation (Ref. 24) of Loh's spectrum (Ref. 23), corresponding to a C_{4v} distorted eightfold cubic center. All numbers are in cm^{-1}.

Main O_h character	This work (O_h')	Experiment (C_{4v}')
$5d(e_g)^1-{}^2E_g$	Γ_{8g} 32630	34200 Γ_7
$5d(t_{2g})^1-{}^2T_{2g}$	Γ_{8g} 50480	50000 Γ_7
	Γ_{7g} 51870	51700 Γ_6
		53500 Γ_7
$6s^1-{}^2A_{2g}$	Γ_{6g} 70080	(70000)[a]

[a]Value corresponding to Ce^{3+} in CaF_2 (Ref. 23).

The agreements with experiments are in the line of previous agreements achieved in similar transitions of materials with simple manifolds, such as $4f$-$5d$ absorptions and emissions of $Cs_2NaYCl_6:Ce^{3+}$ (Ref. 9) and $5f$-$6d$ absorptions and emissions of $Cs_2ZrCl_6:Pa^{4+}$ (Ref. 20), and in materials with complex manifolds, such as $5f$-$6d$ absorptions and emissions of $Cs_2NaYCl_6:U^{3+}$ (Ref. 21), and allows us to insist in that state-of-the-art *ab initio* methods of quantum chemistry, as the ones used here, are nowadays in a position to reliably calculate $4f$-$5d$ absorptions and emissions of lanthanide-doped solids. This claim is in contrast with a recent assertion by Andriessen *et al.*[22] based in their *ab initio* calculations on Ce^{3+} doped in BaF_2 and other ionic hosts. They relaxed the structure around the Ce^{3+} impurities in ground-state DFT calculations with periodic boundary conditions; then, they fixed the resulting Ce-F distance (2.438 Å, not far from our result of 2.471 Å) and performed HF, MP2, MP4, CCSD, and CCSD(T) calculations on a cluster, using Madelung embedding. Although they focused their work on a detailed study of the centroid shift rather than on the individual $4f$-$5d$ excitations in the hosts, they concluded that, in contrast with pre-

vious claims,[9,48] accurate *ab initio* calculations of $4f$-$5d$ excitations of lanthanides in ionic hosts are not possible. We can say that the Ce-F distance they used belongs to the short-distance regime (see the vertical dashed line in Fig. 1), so that their conclusion might be biased by the large anomalies that the insufficiencies of Madelung embedding can create when diffuse orbitals like $5d$ are involved. Let us mention that large anomalies due to the insufficiencies of Madelung embedding are also found in low-symmetry site substitutional defects of lanthanide ions, even in the ground state; a detailed study is underway and will be reported elsewhere.[49] Finally, let us mention that the anomalies due to a wrong embedding shown here for an ion with simple manifolds like Ce^{3+} must be general to the lanthanide and actinide series, which have very complex manifolds, because they affect the molecular orbitals and, in consequence, propagate to the many-electron states.

IV. CONCLUSIONS

By means of CASSCF and CASPT2 culations on the $4f^1$, $5d^1$, and $6s^1$ manifolds of the $(CeF_8)^{5-}$ cluster embedded in BaF_2, without and with spin-orbit coupling, performed with Madelung embedding and with AIMP embedding, we have shown that *ab initio* embedded-cluster calculations on lanthanide ions in ionic solids in which Madelung embedding is used, may suffer dramatic anomalies when diffuse orbitals are involved, like the excited $5d$ and $6s$ orbitals. The anomalies show up in the predicted structural and spectroscopic properties and are basically due to an artifical leak of the excited electron towards the lattice ions that surround the cluster. The deficiencies are corrected when quantum-mechanical embedding effects representing the linear-independency conditions between the cluster and environment wave functions, which are present in AIMP embedding, are taken into account. The $4f$-$5d$ absorption energies calculated with spin-orbit coupling, AIMP embedding, and correlating the electrons with main character F-$2s2p$ and Ce-$4d5s5p4f5d$, show good agreement with experiment. The present results support previous claims that state-of-the-art *ab initio* methods of quantum chemistry as the ones used here are nowadays in a position to reliably calculate $4f$-$5d$ transitions of lanthanide-doped solids. A proper embedding is crucial for this.

ACKNOWLEDGMENT

This work was partly supported by a grant from Ministerio de Educación y Ciencia, Spain (Dirección General de Investigación Grant No. CTQ2005-08550).

*Corresponding author. Electronic address: luis.seijo@uam.es

[1] J. Ehrlich, P. F. Moulton, and R. M. Osgood, Jr., Opt. Lett. **4**, 117 (1979).
[2] P. A. Tanner, C. S. K. Mak, and M. D. Faucher, Chem. Phys. Lett. **343**, 309 (2001).
[3] I. Sokólska and S. Kück, Chem. Phys. **270**, 355 (2001).
[4] C. H. Lu and R. Jagannathan, Appl. Phys. Lett. **80**, 3608 (2002).
[5] M. F. Reid, L. van Pieterson, R. T. Wegh, and A. Meijerink, Phys. Rev. B **62**, 14744 (2000).
[6] B. R. Judd, Phys. Rev. Lett. **39**, 242 (1977).
[7] C. A. Morrison, J. Chem. Phys. **72**, 1001 (1980).
[8] Z. Barandiarán and L. Seijo, J. Chem. Phys. **119**, 3785 (2003).
[9] P. A. Tanner, C. S. K. Mak, N. M. Edelstein, K. M. Murdoch, G. Liu, J. Huang, L. Seijo, and Z. Barandiarán, J. Am. Chem. Soc. **125**, 13225 (2003).
[10] Z. Barandiarán and L. Seijo, J. Chem. Phys. **89**, 5739 (1988).
[11] B. Ordejón, L. Seijo, and Z. Barandiarán, J. Chem. Phys. **119**, 6143 (2003).
[12] J. L. Pascual, L. Seijo, and Z. Barandiarán, J. Chem. Phys. **98**, 9715 (1993).
[13] C. de Graaf, C. Sousa, and R. Broer, J. Mol. Struct.: THEOCHEM **458**, 53 (1999).
[14] M. A. Nygren, L. G. M. Pettersson, Z. Barandiarán, and L. Seijo, J. Chem. Phys. **100**, 2010 (1994).
[15] B. O. Roos, P. R. Taylor, and P. E. M. Siegbahn, Chem. Phys. **48**, 157 (1980); P. E. M. Siegbahn, A. Heiberg, J. Almlöf, and B. O. Roos, J. Chem. Phys. **74**, 2384 (1981); P. Siegbahn, A. Heiberg, B. Roos, and B. Levy, Phys. Scr. **21**, 323 (1980).
[16] K. Andersson, P.-Å. Malmqvist, B. O. Roos, A. J. Sadlej, and K. Wolinski, J. Phys. Chem. **94**, 5483 (1990).
[17] K. Andersson, P.-Å. Malmqvist, and B. O. Roos, J. Chem. Phys. **96**, 1218 (1992).
[18] Z. Barandiarán and L. Seijo, Can. J. Chem. **70**, 409 (1992).
[19] L. Seijo, J. Chem. Phys. **102**, 8078 (1995).
[20] L. Seijo and Z. Barandiarán, J. Chem. Phys. **115**, 5554 (2001).
[21] L. Seijo and Z. Barandiarán, J. Chem. Phys. **118**, 5335 (2003).
[22] J. Andriessen, P. Dorenbos, and C. W. E. van Eijk, Phys. Rev. B **72**, 045129 (2005).
[23] E. Loh, Phys. Rev. **154**, 270 (1967).
[24] W. J. Manthey, Phys. Rev. B **8**, 4086 (1973).
[25] M. Yamaga, S. Yabashi, Y. Masui, M. Honda, H. Takahashi, M. Sakai, N. Sarukura, J.-P. R. Wells, and G. D. Jones, J. Lumin. **108**, 307 (2004).
[26] A. Zaitsevskii and J. P. Malrieu, Chem. Phys. Lett. **223**, 597 (1995).
[27] J. Finley, P.-Å. Malmqvist, B. O. Roos, and L. Serrano-Andrés, Chem. Phys. Lett. **288**, 299 (1998).
[28] S. Huzinaga, L. Seijo, Z. Barandiarán, and M. Klobukowski, J. Chem. Phys. **86**, 2132 (1987).
[29] R. D. Cowan and D. C. Griffin, J. Opt. Soc. Am. **66**, 1010 (1976).
[30] J. H. Wood and A. M. Boring, Phys. Rev. B **18**, 2701 (1978).
[31] R. Llusar, M. Casarrubios, Z. Barandiarán, and L. Seijo, J. Chem. Phys. **105**, 5321 (1996).
[32] G. Karlström, R. Lindh, P. A. Malmqvist, B. O. Roos, U. Ryde, V. Veryazov, P. O. Widmark, M. Cossi, B. Schimmelpfennig, P. Neogrady, and L. Seijo, Comput. Mater. Sci. **28**, 22 (2003).
[33] V. Vallet, L. Maron, C. Teichteil, and J.-P. Flament, J. Chem. Phys. **113**, 1391 (2000).
[34] L. Seijo and Z. Barandiarán, in *Computational Chemistry: Reviews of Current Trends*, edited by J. Leszczyński (World Scien-

tific, Singapore, 1999), Vol. 4, p. 55.
[35] S. Huzinaga and A. A. Cantu, J. Chem. Phys. **55**, 5543 (1971).
[36] S. Huzinaga, D. McWilliams, and A. A. Cantu, Adv. Quantum Chem. **7**, 187 (1973).
[37] *Crystals with the Fluorite Structure*, edited by W. Hayes (Clarendon, Oxford, 1974).
[38] J. Andzelm, M. Klobukowski, E. Radzio-Andzelm, Y. Sakai, and H. Tatewaki, *Gaussian Basis Sets for Molecular Calculations*, edited by S. Huzinaga (Elsevier, Amsterdam, 1984).
[39] T. H. Dunning and P. J. Hay, in *Modern Theoretical Chemistry*, edited by H. F. Schaefer, III (Plenum, New York, 1977).
[40] H. M. Evjen, Phys. Rev. **39**, 675 (1932).
[41] Detailed core and embedding AIMP data libraries in electronic format are available from the authors upon request or directly at the address http://www.uam.es/quimica/aimp/Data/-AIMPLibs.html. See also Ref. 32.
[42] L. Seijo, Z. Barandiarán, and B. Ordejón, Mol. Phys. **101**, 73 (2003).
[43] L. Seijo, Z. Barandiarán, and E. Harguindey, J. Chem. Phys. **114**, 118 (2001).
[44] M. Casarrubios and L. Seijo, J. Mol. Struct.: THEOCHEM **426**, 59 (1998).
[45] P. Dorenbos, J. Lumin. **87-89**, 970 (2000).
[46] X. Cao and M. Dolg, Chem. Phys. Lett. **349**, 489 (2001).
[47] F. Ruipérez, L. Seijo, and Z. Barandiarán, J. Chem. Phys. **122**, 234507 (2005).
[48] Z. Barandiarán, N. M. Edelstein, B. Ordejón, F. Ruipérez, and L. Seijo, J. Solid State Chem. **178**, 464 (2005).
[49] J. Schamps, I. Noiret, F. Real, L. Seijo, and Z. Barandiarán (unpublished).
[50] R. J. Lang, Phys. Rev. **49**, 552 (1936).